Preparation, Characterization and Physical Properties Study of $La_{0.7}Sr_{0.3}Co_{1-x}Fe_xO_{3-\delta}$ Perovskites Prepared by Sol-Gel Method

A.G. Mostafa [1]*, Ibraheem Othman Ali [2], I.M. Ashraf [3] and M.G. Ismaeil [3]

[1.] Phys. Dept., Faculty of Science, Al-Azhar Univ., Nasr City (11884), Cairo, Egypt
[2.] Chem. Dept., Faculty of Science, Al-Azhar Univ.,Nasr City (11884), Cairo, Egypt
[3.] Phys. Dept., Faculty of Science, Aswan Univ., Aswan, Egypt
*drahmedgamal@yahoo.com

Abstract: Some perovskite samples of the composition $La_{0.7}Sr_{0.3}Co_{1-x}Fe_xO_3$ (where x= 0.4, 0.5, 0.6 and 0.8) have been prepared by the sol-gel method. The TGA/DTA analysis indicated that perovskite structure may be formed at about 930 °C, and therefore the obtained powder samples have been calcinated at 1000 °C for 24 h. XRD analysis of all samples indicated that a single perovskite phase has been crystallized in rhombahedral structure and all crystallites are found within the nano-size range. Saturation magnetization (Ms) and reminance magnetization (Mr) were found to increase monotonically with the increase of Fe content while coerctivity field decreased. The dc conductivity was found to increase with increasing temperature where all samples behave like sami-conductors and the small polaron hopping model with thermally activated charge transfer is the applicable conduction mechanism. Also, the optical band gap increased with increasing Fe content.

1. Introduction

Transition metal oxides occupy a wide area of material science now, where they represent the most extensive applied materials. These materials exhibit wide range of properties, from high superconductivity to magneto-resistance phenomena, and they provide a fruitful chance for their investigations. Perovskite structure, particularly, can accommodate different amounts of transition metal oxides, and they characterized by a remarkable level of stability. However, perovskites and their like structural compounds have provided an entire series of technological and theoretical studies [1-4].

Lanthanum-strontium-cobalt-iron (LSCF) perovskites seem to be of particular interest in terms of their possible applications, and they have been extensively studied as potential cathode materials for solid oxygen fuel cells (SOFC) [5–7]. When these cells have operating in an intermediate temperature range (600–800 °C), they overcome major problems, which hinder their commercialization for various technological applications. It was found that lower operating temperatures requires higher activity of electrodes, especially high ionic conductivity electrolyte, low over potential and lower overall internal resistance loss. These requirements can be met by developing new electrode materials, new cell assembly concepts and novel fabrication methods [8-14]. For cathode materials, the occurrence of mixed ionic-electronic conductivity can be highly benefited, as it allows oxygen reduction at the active centers on the entire surface of the cathode material. The oxygen ions can be transported in the whole cathode when non-stoichiometric oxygen exists in the cathode material in the working temperature range [15]. Among many of the possible candidates for SOFC working at intermediate temperature range, perovskite prepared from La–Sr–Co–Fe (LSCF) oxides appeared of special interest. This may be due particularly to their high mixed ionic-electronic conductivity, sufficient catalytic activity towards oxygen reduction and good thermo-chemical compatibility [6, 7 and 15]. It was found also that, LSCF perovskites with higher strontium content prepared at lower temperatures exhibit relatively higher non-stoichiometric oxygen ratio [16].

However, in this article, some $La_{0.7}Sr_{0.3}Co_{1-x}Fe_xO_3$ (x= 0.2, 0.4, 0.5 and 0.8) nano-crystallite perovskits have been prepared by sol-gel method. Then the variation of the crystal structural parameters as well as the corresponding physical properties changes will be investigated extensively as cobalt oxide was gradually replaced by iron oxide.

2. Experimental
2.1. Sample preparation

$La(NO_3)_3.6H_2O$, $Sr(NO_3)_2$, $Co(NO_3)_2.6H_2O$ and $Fe(NO_3)_3.9H_2O$ with purity not less than 99%, were used as a starting materials. These materials were taken in the desired amounts to form a solution in distilled water. First, a saturated aqueous solution of stoichiometric amounts of the respective metal nitrates

are mixed and stirred on a hot plate at about 150 °C. Citric acid and polyvinyl alcohol (PVA) were added slowly to the solution during stirring to yield a gel, where the cations were expected to be statistically distributed in chelate complexes. The formed gel was heated further until solid foam was formed. Such foam was then ground and dried at 200°C overnight. The dried resin was ground and the obtained powders were then washed with distilled water, filtered and dried at 200°C again. The powders were then ground in an agate mortar and then pressed at 300 MPa using a 13 mm diameter cylindrical die. Depending on the TGA/DTA analysis (that will be discussed latter), the obtained pellets were sintered in air at 1000°C for 24 h. The compositions of the obtained solid samples as well as the supposed nominations are exhibited in Table (1).

Table 1. The compositions and the supposed nominations of the prepared samples

Sample no.	Chemical composition	nomination
1	$La_{0.7}Sr_{0.3}Co_{0.6}Fe_{0.4}O_3$	LSCF 7364
2	$La_{0.7}Sr_{0.3}Co_{0.5}Fe_{0.5}O_3$	LSCF 7355
3	$La_{0.7}Sr_{0.3}Co_{0.4}Fe_{0.6}O_3$	LSCF 7346
4	$La_{0.7}Sr_{0.3}Co_{0.2}Fe_{0.8}O_3$	LSCF 7328

2.2. TGA/DTA analysis

The dried gel was then, thermally analyzed applying thermo-gravimetric and differential thermal analysis (TGA/DTA) technique, using NETZSCH STA 449F3 apparatus, in static atmospheric from RT up to 1000ºC. A heating rate of 10ºC/min was applied to determine exactly the optimum calcination temperature of the perovskites under preparation.

2.3. X-ray diffraction analysis

X-ray diffraction (XRD) measurements were carried out using a Bruker D8 Advanced X-ray diffractometer (40 kV, 50 mA, sealed Cu X-ray tube, λ = 1.5406 A˚). Structural refinements has performed using the Rietveld method (as applied in the software package TOPAS), to check the phase purity and to determine the lattice parameters.

2.4. Density measurements

Archimed's technique was applied to obtain experimentally the density values of the solid samples at room temperature after they were calacinated at 1000ºC for 24 h. The used emersion liquid was toluene.

2.5. Magnetic measurements

Magnetic characterization was carried out using vibrating sample magnetometer (VSM) (Lake Shore with sensitivity of 1×10^{-6} emu) and the sample weight was about 20 mg. Hysteresis measurements were made with a magnetic field oscillating between ±12,000 Gauss.

2.6. Electrical measurements

The temperature dependence dc electrical conductivity (σ) of the sintered samples was measured by using the two probe dc technique at temperatures between about 30 and 550°C in air using silver wires and silver paste as contacts with Agilent 4284A LCR Meter Bridge.

2.7. Optical measurements

An ultra violet-Visible (UV-VIS) diffuse reflectance spectrometer (PG Instruments, UK) was used to obtain the optical transmission spectra for the studied perovskite samples, from which the optical band gap values were then calculated.

3. Results and Discussion
3.1. Thermal analysis

The obtained TGA/DTA curve for the sample having the composition ($La_{0.7}0Sr_{0.3}Co_{0.6}$ $Fe_{0.4}O_3$) are shown in Fig. (1) as representative curve, and all samples show approximately similar behavior. From all TGA/DTA curves, it is seen that the total weight loss occurred in three main stages. The first stage appeared at about 130°C, that corresponds the observed endothermic peak at about 132.1°C in the DTA curves. This stage can be attributed to the loss of water of crystallization from $Fe_2O_3 \cdot xH_2O$ and $Co(NO_3)_2 \cdot 6H_2O$, and/or to the evaporation of moisture content present through the nano-crystallite particles. The weight loss in the second stage appeared at about 210°C corresponding to the DTA peak at 208.5°C, which can be attributed mainly to the decomposition of PVA that used during synthesis. The third stage appeared at about 520°C that corresponding to the exothermic peak at 525.7°C, which may be due to the decomposition of the formed metal complexes [17].
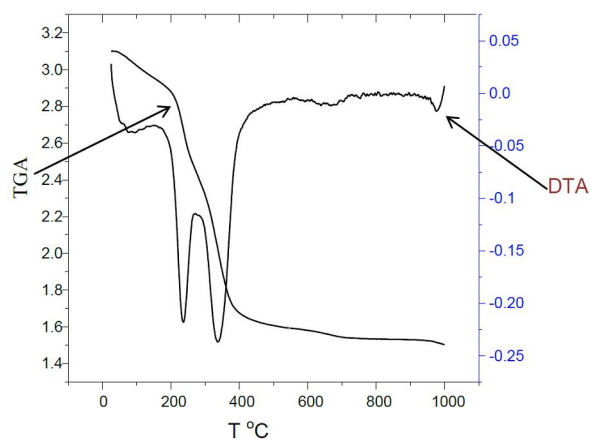
Figure 1. TGA/DTA curves of "$La_{0.7}Sr_{0.3}Co_{0.6}Fe_{0.4}O_3$" dried gel before sintering

An endothermic peak appeared at about 930°C which can be attributed to the complete formation of the prepared perovskite samples [17]. However, the

calcination temperature can evidenced to be about 930°C, as determined from the obtained TGA/DTA curves. Similar behavior has been already reported for other perovskites phase formation at very high temperature [18].

3.2. The XRD analysis

Figure (2) shows the obtained XRD patterns of all the studied perovskite samples. The obtained results reveal that the main phase obtained is a single perovskite phase, in addition to very slight amounts of unreacted oxides, within the limits of errors. It is observed also that, all samples show rhombohedral structure as the main structural phase.
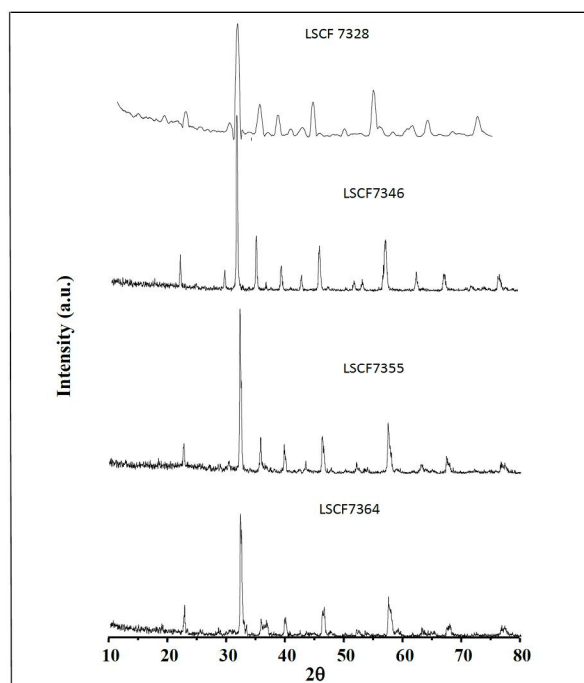
Figure 2. XRD patterns of $La_{0.7}Sr_{0.3}Co_{1-x}Fe_xO_3$ (x = 0.4, 0.5, 0.6 and 0.8) nano-crystallite perovskites calcinated at 1000°C for 24 h

It was reported early that crystallographic perovskite phase contained La FeO_3, Fe_3O_4 and Co_3O_4 as impurity even after sintering at 1250°C for about 4 or 6 h [19]. From the obtained XRD patterns, the lattice parameters, crystal size and cell volume are calculated and the obtained values are listed in Table (2).

From the obtained XRD results, it is seen that, as the iron content was gradually increased at the expense of cobalt content, the crystallite size and cell volume show very slight gradual increase. Such increase may be due to the differences between the volumes of both Co and Fe cations. The variation of both the crystallite size and cell volume are presented graphically in Fig.s (3 & 4) respectively. Slight broadening has been also observed in all the obtained

XRD patterns of the studied samples, which indicated generally that, all crystallites are in the nano-size. Also, the slight variations in the peak intensities and positions may indicate very slight distortion in the structure, which in turn may be due to the differences between both iron and cobalt as well as the differences in the non-oxygen stoichiometry in the studied samples.

Table 2. Lattice parameters, cell volume and crystallite size of the studied perovskites

Sample Nomination	Lattice parameters (A°)	Crystallite size (nm)	Cell volume (A°³)
LSCF 7364	a = 5.443 c = 13.221	28.5	391.689
LSCF 7355	a = 5.453 c = 13.232	29.2	393.456
LSCF 7346	a = 5.459 c = 13.239	30.1	394.531
LSCF 7328	a = 5.471 c = 13.251	30.8	396.627
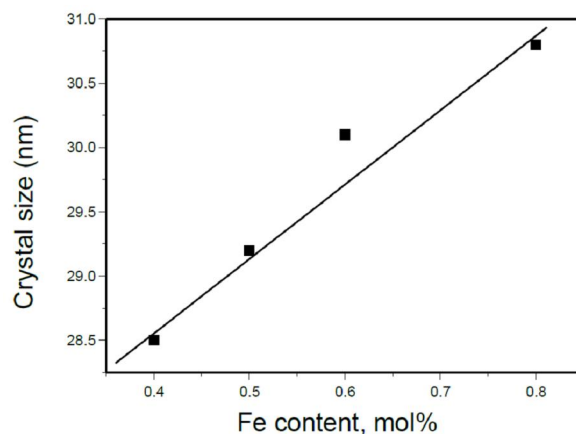
Figure 3. The variation of the crystallite size as a function of Fe content
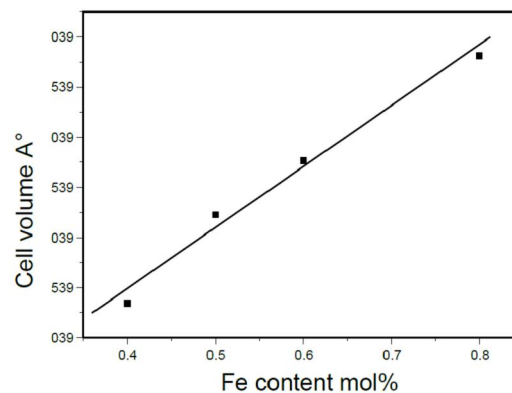
Figure 4. The variation of the cell volume as a function of Fe content

3.3. Density measurements

The density values were obtained applying Archimedes technique using toluene as an emersion liquid. The obtained densities are exhibited in Table (3), where it appeared that as iron content was gradually increased in the studied samples, the density shows very slight gradual decrease. This may be due to some slight gradual increase in the porosity of the studied samples [4]. This was found in agreement with the variation of the calculated lattice parameters, crystallite size and cell volume.

Table 3. The obtained density values of the studied samples

Sample number	nomination	Archimedes' density g.cm^{-1}
1	LSCF 7364	6.26
2	LSCF 7355	6.25
3	LSCF 7346	6.22
4	LSCF 7328	6.18

3.4. Magnetic properties

The vibrating sample magnetometer (VSM) was used here to measure the magnetic properties of the studied perovskite samples. The vibrating magnetic field was between ±12,000 Gauss, applied perpendicular to the sample under measurement, and the obtained hysteresis loops are presented in Fig. (5). The calculated magnetic parameters (saturation magnetization (Ms), remnant magnetization (Mr) and the coercivity field (Hci)), are presented in Table (4).

From this table, it can be seen that, as iron cations were gradually increased at the expense of cobalt cations, Ms and Mr exhibit an increasing trend, while Hci exhibits a gradual decrease. Figure (6) shows the variation of the saturation magnetization (Ms) as a function of Fe content, where it exhibits approximately gradual linear increase.
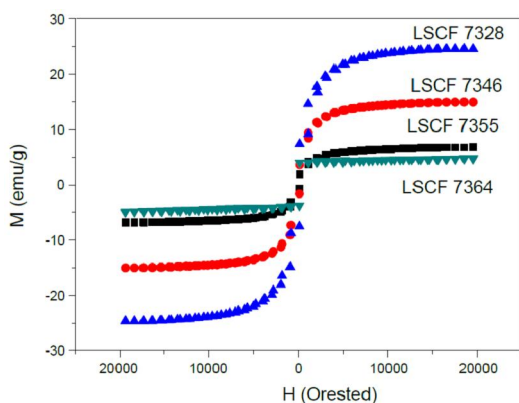
Figure 5. RT (M–H) Hysteresis loops of all the studied samples

Table 4. The obtained magnetic constants (Coercively field (Hci), Saturation magnetization (Ms), and Remanence magnetization (Mr))

Nomination	Hci	Ms	Mr
LSCF 7364	263.61	4.813	1.1800
LSCF 7355	260.54	14.987	2.5982
LSCF 7346	255.872	24.646	6.8632
LSCF 7328	248.876	29.651	8.482

It can be concluded from the shapes of the hysteresis loops as well as the calculated magnetic parameters, that all LSCF samples exhibit soft ferromagnetic behavior [20, 21]. That is there are no effects of super-paramagnetic particles on the shapes of the obtained hysteresis, which may be due to the close resemblance between cobalt and iron cations. Also it can be supposed that some nano-sized magnetic grains have been created in the studied perovskites matrices with considerable concentration of vacancies which act to create magnetic defects [22].

Figure (6) shows the variation of Ms as a function of Fe content, where it exhibits approximately gradual linear increase as iron was gradually increased.
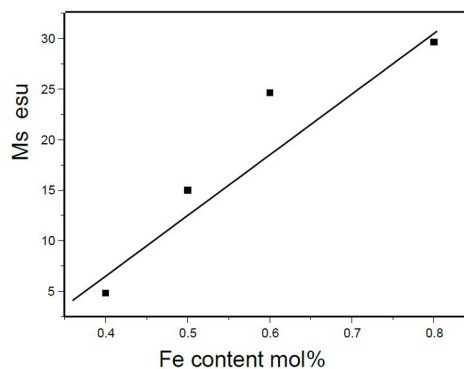
Figure 6. The variation of Ms as a function of iron content

3.5. DC Electrical conductivity

The dc conductivity of LSCF perovskites is well characterized by their mixed ionic-electronic conduction properties [15]. However, the dc electrical conductivity of the studied perovskite samples has been measured in the temperature range from RT up to 550°C. Fig. (7), represents the variation of lnσ with the reciprocal of temperature. It can be observed easily that all samples show two straight lines intersected in the temperature range from about 400 to 415°C for all samples. These two straight lines can be taken as evidence for the occurrence of both ionic and electronic conductivities [23]. It is appeared also that all samples show a gradual increase of conductivity with temperature, over the investigated temperature

range, and the obtained straight lines obey an Arrhenius type equation

$$\sigma = \sigma_o \, exp\left(\frac{\Delta E}{k_B T}\right)$$

where, σ, σ_o, ΔE, T and k_B are the temperature dependent conductivity, pre-exponential factor, activation energy, absolute temperature and Boltzmann constant respectively.

Since the conductivity shows gradual increase with temperature, therefore it is a thermally activated process and these perovskites behave like semiconductors in the examined temperature range. However it can be supposed that the dc conductivity may be due to the hopping of electrons between the present transition metal cations (iron-iron, cobalt-cobalt and iron-cobalt) as well as the oxygen anion vacancies in the perovskite matrices [24, 25]. That is, it can be supposed that there are two kinds of charge carriers (electrons and ions) in the studied perovskite samples. The obtained conductivity results and the observed behavior are similar to those reported in some literature [26, 27]. It can be supposed also that in these materials, the conductivity is controlled by small polaron hopping model with thermally activated charge transfer [28].
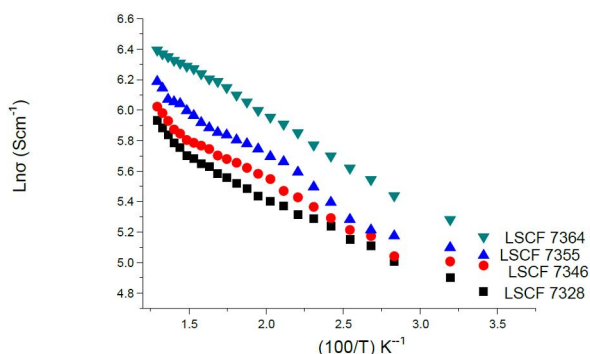
Figure 7. Arrhenius plots of $La_{0.7}Sr_{0.3}Co_{1-x}Fe_xO_3$ perovskite samples

Dutta et al has observed a decrease in conductivity with increasing temperature, indicating a metallic conducting behavior of LSCF perovskite samples with low Fe content [28]. This is consistent with the fact that the degree of the non-stioshiomtric oxygen deficiency is higher in these LSCF compositions with high Co content. For samples with higher Fe content it is also possible to observe such like behavior, but at higher temperatures (above 900°C) due to the decrease in the concentration of electron hole pairs, where the concentration of oxygen vacancies increased [25].

Based on the above studies, the variation of the dc conductivity as a function of Fe content has been exhibited in Fig. (8), at three fixed temperatures (350,

450 and 550°C), where a gradual linear decrease is clearly observed. This observation may be due to the gradual increase of iron at the expense of cobalt where this replacement acts to decrease the density and increase the cell volume of the studied samples. This main that such replacement increases the matrices porosity which in turn may decrease the electron hopping between cobalt and iron cations.
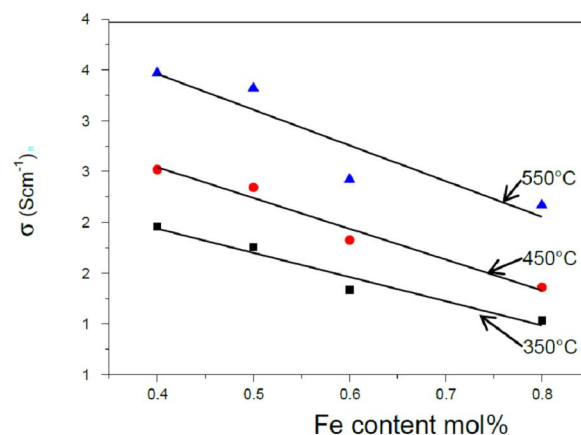
Figure 8. The variation of σ (Scm^{-1}) with Fe content at three fixed temperature

The electrical activation energies of the studied samples were then calculated from the slopes of the straight lines at higher temperatures, and the obtained values are exhibited graphically in Fig. (9). It is seen that the electrical activation energy increased gradually with the gradual replacement of cobalt by iron which is consistent with the obtained data about the σ_{dc} with iron content (see Fig. (7)). Also, these results are found in complete agreement with those reported previously by Kostogloudis et al [25] and Dutta et al [28].
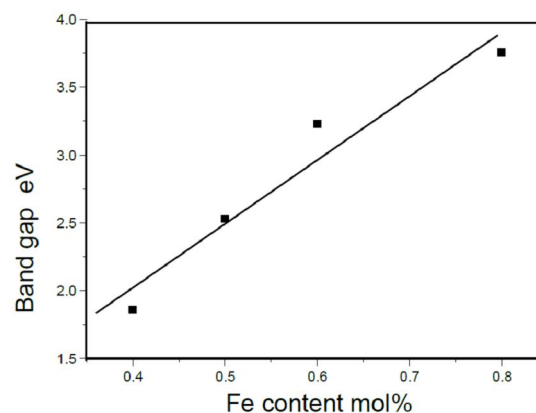
Figure 9. The variation of the electrical activation energy as a function of iron content

It appeared from this figure that ΔE increased gradually from 1.86 eV for the sample nominated

LSCF 7364 up to 3.76 eV for the sample nominated LSCF 7328. This may be due to the increase of porosity of the studied perovskite samples as cobalt cations were gradually replaced by iron cations.

3.6. Optical properties

The study of the fundamental absorption edge in the UV-VIS region represents an interesting method for the optical transitions and electronic band structure in crystalline and non-crystalline materials. Fig. (10) shows the relation between the photon energy ($h\upsilon$ eV) and $(\alpha h\upsilon)^{1/2}$, for the samples containing 0.4 and 0.8 mol % iron cations. This plot is usually known as Tauc plot [29, 30]. From such figure the optical band gap of the studied samples can be calculated, and the obtained values are then plotted in Fig. (11) as a function of iron content. It appears that the band gap values increased gradually from 1.92 up to 3.2 eV for the samples containing 0.4 and 0.8 mol % Fe respectively. This behavior was found in agreement with the behavior of the electrical band gap, (see Figure (9)).
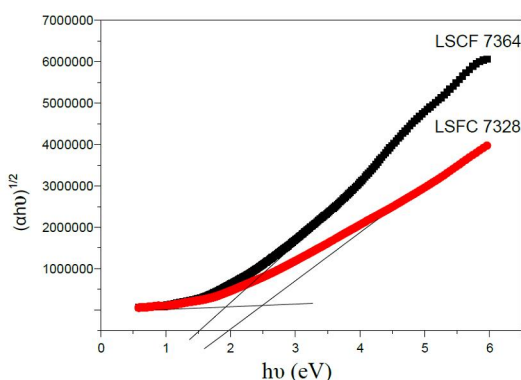
Figure 10. Tauc plot of selected perovskite samples, as representative curve
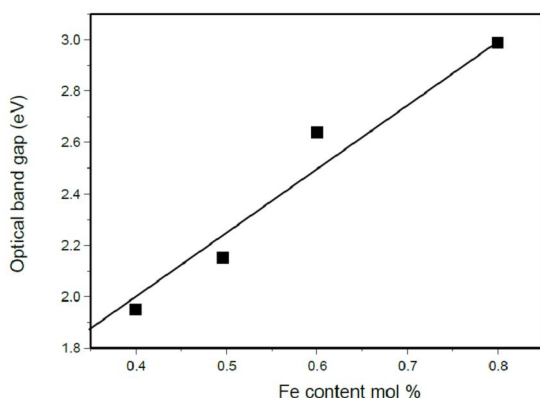
Figure 11. The variation of the E_{gap} as a function of Fe content

Korotin et al [31], have calculated theoretically the band gap in $LaCoO_3$ considering rhombohedral distorted phase, where they could estimate a direct

transition band gap of 2.07 eV. When Sr^{2+} partially substitutes La, in the absence of Fe^{2+}, no appreciable change in the band gap was observed. It was found also that the presence of Fe^{2+} can modify the absorption properties of lanthanum-cobalt perovskite, and the sample LSCF6428 that contained the higher amount of Fe showed the highest value of band gap (3.2 eV). This wide band gap can be related to less significant oxygen lattice defects [32]. It can supposed also that, the observed differences in the band gap values between the LSCF samples are related to slight differences in the crystallite size as well as the differences in the electronic band structure due to the created oxygen vacancies.

4. Conclusion

$La_{0.7}Sr_{0.3}Co_{1-x}Fe_xO_3$ (x= 0.4, 0.5, 0.6 and 0.8) have been successfully prepared by the sol-gel method, and clasinated at 1000^oC for 24 h. The calsind pellets were then thoroughly investigated. It can be concluded that a rhombohedral crystallographic perovskites phase has been obtained, where the crystallites of all samples are found in the nano-size and as iron content was gradually increased the lattice parameters, crystallite size and cell volume show slight gradualincrease.

According to the dc conductivity measurement, it can be concluded that the conductivity increased with temperature and the conduction mechanism may be thermally activated charge transfer. The electrical activation energy increased with the increase of iron content and the obtained values showed that all samples exhibit semiconducting behavior.

From the magnetic characterization, the saturation magnetization M_s and remenance magnetization increased with increasing Fe content while coercivity field decreased. The optical band gap increased also with the increase of Fe content, so the photoreactivity decreased by increasing Fe content.

Corresponding Author:
Prof. Dr. Ahmed G. Mostafa
Department of Physics
Faculty of Science
Al-Azhar University, Nasr City, Cairo, Egypt
E-mail: *drahmedgamal@yahoo.com

References
1. A. Navrotsky and D. Weidner, J. Geophys. Monograph., 45 (1989) 27.
2. M. W. Lufaso, P. M. Woodward and J. Goldberger, J. Solid State Chem., 177 (2004) 1615.
3. P. M. Woodward, PhD thesis, Oregon State University, "Structural distortion, phase

transitions, and cation ordering in the perovskite and tungsten trioxide structures"(1996).

4. A.G. Mostafa, S.A. Mazen and A. El-Attar, Nature & Science, 12 (2) (2014) 112.

5. A. Esquirol, N.P. Brandon, J.A. Kilner and M. Mogensen, J. Electrochem. Soc., 151 (2004) 1847.

6. A. Petric, P. Huang and F. Tietz, Solid State Ionics, 135 (2000) 719.

7. E. Maguire, B. Gharbage, F.M.B. Marques and J.A. Labrincha, Solid State Ionics, 127 (2000) 329.

8. N.Q. Minh, J. Am. Ceram. Soc., 76 (1993) 563.

9. A. Boudghene Stambouli and E. Traversa, Renew, Sustain. Energy Rev., 6 (2002) 433.

10. E. Ivers-Tiffee, A. Weber and D. Herbstritt, J. Eur. Ceram. Soc., 21 (2001)1805.

11. H. J. Hwang, J. W. Moon, S. Lee and E. A. Lee, J. Power Sources, 145 (2005) 243.

12. Y.J. Leng, S.H. Chan, S.P. Jiang and K.A. Khor, Solid State Ionics, 170 (2004) 9.

13. Q.L. Liu, K.A. Khor and S.H. Chan, J. Power Sources, 161 (2006) 123.

14. J. Yan, H. Matsumoto, M. Enoki and I. Shihara, Electrochem. Solid-State Lett., 8 (2005) 389.

15. S. B. Adler, J. A. Lane and B. C. H. Steele, J. Electrochem. Soc., 143 (1996) 3554.

16. S. J. Skinner, Int. J. Inorg. Mater., 3 (2001) 113.

17. J.W. Stevenson, T.R. Armstrong, R. D. Carneim, L.R. Pederson and W.J.Weber, J. Electrochem. Soc., 143 (1996) 2722.

18. Z. D. Zivkovic, D. T. Zivkovic, and D. B. Grujicic, J. Therm. Anal., 53 (1998) 617.

19. X. Yan, J. Chen, Y. Qi, J. Cheng and Z. Meng, J. Eur. Ceram. Soc., 30 (2) (2010) 265.

20. L. Jiangong, X. Kau, Y. Qin and H. Haiying, Phys. Status Solidi (A), 191 (2002) 255.

21. A. G. Mostafa, E. K. Abdel-khalek, W. M. Daoush and M. Y. Hassan, Hyperfine Interact., 184 (2008) 167.

22. M. Pissas, G. Kallias, K. Devlin, A. Simopoulos and D. Niarchos, J, Appl. Phys., 81 (1997) 5770.

23. K. Cherif, J. Dahahri, E. Dahahri, M.Qumezzine and H. Vincent, J. Solid State Chem., 163 (2002) 466.

24. L.W. Tai, M.M. Nasrallah and H.U. Anderson, Solid State Chem., 118 (1995) 117.

25. G. C. Kostogloudis, and Ch. Ftikos, Solid State Ionics, 126 (1999) 143.

26. P. Zeng, R. Ran, Z. Chen, H. Gu, Z. Shao and Diniz da Costa JC, J Membr. Sci., 302 (2007) 171.

27. K. K. Hansen and K.V. Hansen, Solid State ionics, 178 (2007) 1379.

28. A. Dutta, J. Mukhopadhyay and R. N. Basu, J. Eur. Ceram. Soc., 29 (2009) 2003.

29. J. Tauc, Mater. Res. Bull., 5 (1970) 37.

30. A. M. Abdel-Ghany, A. A. Bendary, T. Z. Abou-Elnasr, M. Y. Hassaan and A. G. Mostafa, Nature Science, 12 (6) (2014) 139.

31. M. Korotin, S.Y. Ezhov, I. Solovyev, sV. Anisimov, D. Khomskii and G. Sawatzky, Phys. Rev. (B), 54 (1996) 5309.

32. M. Bradha, T. Vijayaraghavan, S. P. Suriyaray, R. Selvekumar and A.s M. Ashok, J. Rare Earth, 33 (2) (2015) 160.

10/25/2016